Eur. Phys. J. A (2019) **55**: 249
DOI 10.1140/epja/i2019-12890-3

THE EUROPEAN PHYSICAL JOURNAL A

Regular Article – Theoretical Physics

Collective enhancements in nuclear level densities*

Thomas Døssing[1,a] and Sven Åberg[2]

[1] The Niels Bohr Institute, University of Copenhagen, Copenhagen, Denmark
[2] Mathematical Physics, Lund University, Lund, Sweden

Received: 6 May 2019 / Revised: 12 September 2019
Published online: 5 December 2019

Communicated by N. Alamanos

Abstract. Contributions to the nuclear level density from a deformed core and from surface vibrations are discussed. The influence of symmetries of the nuclear shape is highlighted by quoting and discussing analytic Fermi gas level densities for irregular, deformed and spherical shapes. A thorough evaluation of the *rotational enhancement factor* to the level density is carried out for 17 well deformed rare-earth nuclei. Counted experimental levels are compared to levels obtained from the combinatorial level-density model, applying the Folded-Yukawa potential with BCS quasiparticle paring. It is found that the phase space of the rotating core contributes fully to the level density at the low energies where reliable information of experimental levels exists. The analysis is inspired by recent thermal Shell Model Monte Carlo results, which are also included in the comparison. The situation at the neutron excitation energy is also discussed, together with the conditions for vibrational enhancement. Experiments aimed at investigating the fade-away of collective enhancements are briefly discussed.

1 Introduction

Pier-Fransesco Bortignon in his pioneering work together with Ricardo Broglia on the spreading width of giant vibrations [1] describes the coupling of the basic coherent one-particle-one-hole state, that is the vibration, to the next stage, two-particle-two-hole states, including correlations. A proper description of this coupling requires careful consideration of the phases of coupling matrix elements. Eventually, the next stage states are coupled to more involved excitations, and the giant vibration is finally spread over all nuclear levels of the same angular momentum and parity as the vibration, within the envelope of a rather featureless strength function.

The present paper addresses the density in energy of these nuclear levels of the final stage of coupling. At this final stage, the whole available phase space of the nucleus comes into play. Especially, we shall pay attention to the degrees of freedom associated with the dynamic nuclear shape, occurring as surface vibrations and rotations.

All descriptions of nuclear level densities are based on the nuclear shell model in various versions. Many-particle-many-hole excitations in these shell models make up the bulk of the nuclear level density. The addition of collective states such as the vibrations and rotations to the ensemble of many-particle-many-hole states is denoted *collective enhancement* of the level density.

With increasing energy of the nucleus, the problem of *overcounting* arises. For example, low-lying surface vibrations consist of coherent particle-hole states. For an excited nucleus, several incoherent thermally excited particle-hole states are activated. Eventually, with increasing excitation energy, the particle-hole combinations of the surface vibrations will be exhausted by the incoherent excitations, and should not be counted when evaluating the level density.

Thus, the collective enhancement of the level density is expected to *fade away* with increasing excitation energy.

The main topic of the present paper is the rotational enhancement of the level density. First, we shall discuss how the symmetry of the nuclear potential is decisive for the level density. This will be illustrated with schematic evaluations of the level density, based on known Fermi gas expressions. Secondly, we shall evaluate the amount of rotational enhancement in rare-earth nuclei, comparing data to calculations based on the Folded Yukawa potential with BCS and schematic rotational bands added.

The present analysis is inspired by the evaluations of level densities based on large-scale shell-model calculations, in the framework of the auxiliary-field method, with Monte-Carlo sampling governed by a thermal ensemble, abbreviated SMMC [2–4].

* Contribution to the Topical Issue "Giant, Pygmy, Pairing Resonances and Related Topics" edited by Nicolas Alamanos, Ricardo A. Broglia, Enrico Vigezzi.

[a] e-mail: dossing@nbi.ku.dk

For a general reference to level densities, the reader is encouraged to consult a recent review [5], wherein level densities are discussed for a wide range of nuclei and excitation energies.

Section 2 of the present paper provides an introduction to level densities of spherical and deformed nuclei, giving the different views on the *rotational enhancement of the level density*.

Section 3 presents a general discussion of the different versions of the Fermi gas level density which are relevant, emphasizing the symmetry of the nuclear shape.

Sections 4 and 5 present a careful evaluation and discussion of the rotational enhancement of the level density at the lowest excitation energies of well-deformed nuclei, on the basis of experimental as well as calculated nuclear states.

Section 6 provides a short discussion of the situation at the neutron separation energy, where also precise information about the level density exists. Also, possible vibrational enhancement is discussed together with recent experiments aimed at determining the behavior of enhancements of the level density above the neutron separation energy.

Section 7 gives a short conclusion.

2 Rotational enhancement of level density

When discussing the level density of excited nuclei, it is important to consider the rotational symmetry, and the associated conservation of angular momentum.

The first realistic expression for the nuclear level density, based on the Fermi gas, was proposed by Bethe [6, 7], and is derived assuming coupling of single-particle angular momenta to form the total angular momentum of the nucleus. Later, Ericson [8] pointed out that for deformed nuclei, the level density should address states with the strong coupling scheme for angular momentum. The single-particle orbits in the deformed potential add up their projections of angular momentum on the symmetry axis to the intrinsic projection, which is then combined with the angular momentum of the collective rotor.

As pointed out by Bjørnholm, Bohr and Mottelson [9], the strong coupling scheme of the angular momentum, in the Ericson formulation, leads to a level density which is much larger than the level density obtained by only coupling the nucleon angular momenta. This *enhancement of the level density of deformed nuclei* arises from the extension of the phase space by the rotational degrees of freedom of a deformed rotor. One should note that the enhancement of the level density already appears for angular momentum $I = 0$ or $I = 1/2$. The first realistic level densities of nuclei evaluated on the basis of nuclear single-particle potentials and thermal BCS pairing largely confirmed the enhancement [10,11].

Still, the deformed rotor is made out of coherent nucleonic excitations, as described by Belyaev and Zelevinsky [12]. The role of specific components of the residual interaction in generating rotational bands, as well as the consequences for rotational enhancement have recently been discussed by Karampagia *et al.* [13].

At higher energy the deformed core should not be able to contribute extra degrees of freedom. Consequently, the rotational enhancement should gradually fade away with increasing excitation energy, as also predicted by Bjørnholm, Bohr and Mottelson.

This topic was addressed more specifically by Hansen and Jensen in theoretical calculations applying the Elliot model [14]. For the level density of well-deformed rare-earth nuclei, they found a temperature inversion covering a quite wide interval in excitation energy, from about 30 MeV to 60 MeV, that is an increasing temperature up to around $T = 1.9$ MeV with excitation energy from 0 to 30 MeV, followed by a drop and then increase again, reaching $T = 1.9$ MeV at 60 MeV. If one could keep an ensemble of such nuclei in a heat bath, prohibiting their decay, one would observe a first order phase transition at temperature $T = 1.9$ MeV with a large latent heat of 30 MeV per nucleus.

Experimentally the temperature inversion should reveal itself in the spectra of evaporated particles. The slope of evaporation spectra are basically given by the inverse temperature, when displayed on a logarithmic plot. If the level density of the nucleus includes such a temperature inversion, the slope should then stay fairly constant, independent of the beam energy in fusion-evaporation reactions. However, in a careful experiment a steadily decreasing slope of the evaporated alpha particles with increasing beam energy was found by Komarov *et al.* [15]. So no fading away of a rotational enhancement was observed.

It has been speculated that large shape fluctuations of nuclei at high excitation energy bring very elongated shapes into play, and for such elongated shapes the rotational enhancement of the level density should remain to much higher excitation energies, thus preventing the fading away of the rotational enhancement altogether [16].

It should be mentioned that an experiment investigating the survival probability against fission of highly excited exotic nuclei was analyzed with level densities including rotational enhancement and fade-away [17]. A rather fine accordance with data was obtained. However, for these nuclei, it seems difficult to distinguish between effects of the shell structure around neutron number $N = 126$, and effects of the rotational enhancement.

We shall here address the rotational enhancement at much lower excitation energies.

Primarily, the rotational enhancement of the level density is defined as the ratio between the Ericson and Bethe level densities for a given nucleus. However, the deformation of nuclei is determined by the shell structure of single particle states in the nuclear potential, which also has large influence on the level density. One cannot force deformed nuclei to be spherical or spherical to be deformed. Even if one could in actual nuclei, the shell effect would probably overshadow the influence of the rotational enhancement.

A better theoretical approach, suggested some years ago by Alhassid and coworkers [2], is based on the shell model, sampling states in a canonical ensemble.

A canonical sampling of states corresponds to contact with a heat bath, and all states will be explored, without regard to symmetries, quantum numbers and degeneracies of levels. To compare to data, a grid in temperature T yields a grid of average energy E. The relevant physical quantity is *the state density*. For a given nucleus of neutron number N proton number Z and energy E, the state density is the sum over the level density of all angular momenta I, weighted by the degeneracy $2I+1$

$$\rho_{state}(E,N,Z) = \sum_I (2I+1)\rho_{level}(E,N,Z,I). \qquad (1)$$

In ref. [2], the enhancement is evaluated as the ratio between the overall state density and the intrinsic state density. It turns out (see sect. 4.1 below), that this ratio, defined for a given deformed shape, yields the deformation enhancement.

The overall state density is obtained by sampling states with the SMMC —Shell Model Monte Carlo technique, and the intrinsic state density is obtained by HFB — Hartree-Fock Bogoliubov, with the same basic energies and interactions as applied in the SMMC calculations.

For light rare-earth nuclei, Alhassid and coworkers found a transition to spherical shape at an excitation energy of about 30 MeV, accompanied by a fading away of the rotational enhancement. The magnitude of the rotational enhancement was found to be much smaller [2] than as predicted by Bjørnholm, Bohr and Mottelson [9], indicating that the excitations contributing to rotational motion are to a substantial degree intermixed with the thermal excitations of nucleons already at quite low excitation energy.

Basically, the question of rotational enhancement of the level density is related to the symmetry of the nuclear shape, and in the next section, we shall illustrate this aspect by quoting and discussing Fermi gas expressions for the level density.

3 Fermi gas expressions

Analytic expressions for the level density can be derived for a Fermi gas with uniform spectra of both protons and neutrons.

3.1 State density, potentials without symmetry

Applying the Laplace transform with the saddle point approximation for excitations in a potential with equidistant levels, one can derive [18] the following expression for the state density of a nucleus with N neutrons, Z protons, and excitation energy E:

$$\rho_{state,np}(N,Z,E) = \frac{\sqrt{\pi}}{12}\frac{1}{(aE)^{1/4}}\frac{1}{E}\exp\left(2\sqrt{aE}\right), \qquad (2)$$

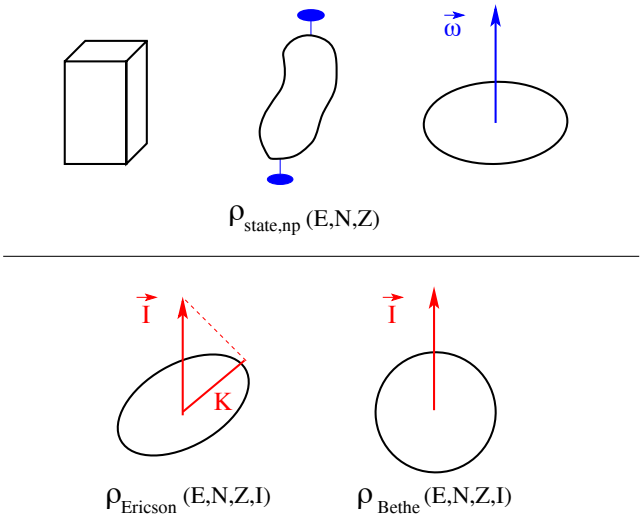

Fig. 1. Illustration of the different symmetries of potentials of Fermion systems, giving rise to different level densities. Top row: With potentials possessing only discrete symmetries, the state density is explored, such as is the case for (i) a box with different lengths (ii) an irregular shape fixed in space, and (iii) a shape forced to rotate at a fixed rotational frequency. Bottom row left: for a deformed shape, rotational bands appear, and the Ericson expression for the level density is relevant. Bottom row right: For a spherically symmetric potential, only nucleonic excitations appear, and the Bethe expression should be applied.

where the subscript "*np*" specifies that exclusively many-particle-many-hole excitations of neutrons and protons contribute to the level density. The expression (2) only contains one parameter, *the level density parameter* a, which is proportional to the sum of densities g_N and g_Z of single particle energies of the two kinds of nucleons in the potential:

$$a = \frac{\pi^2}{6}(g_N + g_Z) \qquad (3)$$

and it is assumed that g_N and g_Z are not too different. The *temperature* is given by

$$T = \sqrt{\frac{E}{a}}. \qquad (4)$$

The same expression (2) can be derived by treating the nucleus as a two-fermion system embedded in a heat bath of temperature T, with average neutron and proton numbers, described by a grand-canonical partition function. The numerator in the level density (2) is the exponent of the entropy, and the denominator is the effective volume in the N-Z-E space occupied by the grand-canonical ensemble, providing a normalization to specific values of N, Z and E.

This state density $\rho_{state,np}(N,Z,E)$ would be observed for nucleons in a nuclear potential without symmetry, or with discrete symmetries such as rotations by angle π. Discrete symmetries will result in degeneracies of the order of 2. Such potentials are illustrated on the upper row of fig. 1, for example the shape in the middle, an irregular

shape fixed in space, symbolically denoted by the blue nails on the figure.

3.2 Cranking model level density

In a rapidly rotating nucleus, illustrated on the right-hand side of the top row of fig. 1, the potential may only have a discrete symmetry, and the angular velocity vector plays the role of the blue nails. This was pointed out by Åberg [19]. Each state of the rotating potential lies on a rotational band. The relevant level density will be the expression for the state density (2), with a factor of 1/2 for symmetry by rotation of angle π around the angular velocity vector:

$$\rho_{cranking}(N,Z,E,I) = \frac{1}{2}\frac{\sqrt{\pi}}{12}\frac{1}{(aE^*)^{1/4}}\frac{1}{E^*}\exp\left(2\sqrt{aE^*}\right) \tag{5}$$

with

$$E^* = E - E_{yrast}(I) \tag{6}$$

being the energy above the yrast line —that is the energy available for nucleonic excitations.

Sampling γ-transitions covering two units of angular momentum, as appearing in the ridges [20] of non-resolved transitions, the factor $\frac{1}{2}$ should be omitted. With a fluctuation analysis of non-resolved transitions [21], one has determined the effective number of unmixed bands above yrast for a few cases of well-deformed rare-earth nuclei, confirming the application of the cranking model level density [21,22].

3.3 Level density of symmetric potentials

The cranking model level density of rapidly rotating nuclei is a special case. For small angular momenta, one cannot avoid taking into account the full rotational symmetry and the associated conservation of angular momentum, both when discussing counted levels, as we shall do here, and when describing compound nucleus reactions.

The first step in taking into account the angular momentum is to add a constraint for the *projection* K of the angular momentum on a symmetry axis. This axis can be along any direction of a spherical shape, or it can be the symmetry axis of a deformed shape. This can mathematically be carried out by means of an extra dimension in the Laplace transform [18]. Keeping to low values of the angular momentum, one obtains a Gaussian distribution in K:

$$\rho_{proj}(N,Z,E,K) = \frac{1}{\sqrt{2\pi}\sigma_K}\exp\left(-\frac{K^2}{2\sigma_K^2}\right)\rho_{state,np}(E,N,Z) \quad \text{for low } K. \tag{7}$$

The variance σ_K^2 in the projection K is given by the temperature times the *moment of inertia* relative to the symmetry axis. This moment of inertia is proportional to the average square of the available single particle projections k of angular momentum:

$$\sigma_K^2 = T\mathcal{J}_\parallel \quad \text{with } \mathcal{J}_\parallel = (g_N + g_Z)\langle k^2\rangle.$$

For independent particle motion, as in the Fermi gas model, $\mathcal{J}_\parallel$ attains the value of the *rigid-body moment of inertia* of the density distribution of neutrons and protons moving in the potential [18].

The final step is to include the size I of the angular momentum vector, and this proceeds on different routes for spherical and deformed nuclei.

3.3.1 Spherical nuclei, the Bethe formula

For a spherical nucleus, only nucleonic excitations are available, and the projection of I is on an external axis, usually denoted by the letter M. Thus, to remind of this interpretation of the axis in this case, one should replace K in the expression (7) with M. With this interpretation, the level density for a given projection M encompasses all angular momenta equal to or larger than M, that is $I = M, M+1, \cdots$. Going one unit up in M (to $M+1$), one looses the angular momentum $I = M$. Thus, the level density at angular momentum I is given as the difference between two neighboring values of the level density with given projection —that is the Bethe formula:

$$\begin{aligned}&\rho_{Bethe}(N,Z,E,I) = \\ &\rho_{proj}(N,Z,E,M=I) - \rho_{proj}(N,Z,E,M=I+1) \\ &\simeq -\frac{\mathrm{d}}{\mathrm{d}M}\rho_{proj}(N,Z,E,M)\Big|_{M=I+1/2}.\end{aligned}$$

One only differentiates the exponential function, neglecting the weaker dependence through the power law in front, yielding

$$\rho_{Bethe}(N,Z,E,I) \simeq (2I+1)\frac{1}{\sqrt{8\pi}\sigma_M^3}\exp\left(-\frac{I(I+1)}{2\sigma_M^2}\right) \times\rho_{state,np}(E,N,Z), \tag{8}$$

where the variance in the projection M is determined by the moment of inertia of the spherical shape, as required by the spherical symmetry

$$\sigma_M^2 = T\mathcal{J}_{sphere}.$$

3.3.2 Deformed nuclei, the Ericson formula

For a deformed nucleus, we only discuss the case of a deformation with a symmetry axis. The angular momentum projection K of ρ_{proj} is then the projection on that axis. Each state counted in ρ_{proj} will in the deformed nucleus act as a band-head of a rotational band with energy:

$$E_{band}(I,K) = \frac{\hbar^2}{2\mathcal{J}_\perp}\left(I(I+1) - K^2\right),$$

where $\mathcal{J}_\perp$ denotes the moment of inertia of the collective rotor perpendicular to the symmetry axis.

The level density at a given angular momentum I should encompass these bands with K in the interval between $-I$ and I. For the nuclei we shall consider here, the nuclear potential and the nuclear density display r-symmetry, that is invariance with respect to a rotation by angle π around an axis perpendicular to the symmetry axis. Such point-symmetries reduce the level density, in this case by a factor of $\frac{1}{2}$, since states with projections K and $-K$ combine to form one band-head. Special care is taken for so-called $r = 0$ bands of $K = 0$ with only particles excited in time-reversed orbitals, for which only even values of I occur. $r = 0$ bands can only exist in even-Z-even-N nuclei [23].

Inserting the band energies, and approximating the level density by a local temperature approximation for changes ΔE in energy

$$\rho(E - \Delta E) \approx \exp\left(-\frac{\Delta E}{T}\right)\rho(E),$$

one ends up with the Ericson expression

$$\rho_{Ericson}(N, Z, E, I) \simeq \frac{1}{\sqrt{2\pi}\sigma_K}\left\{\sum_{K=-I}^{K=I}\frac{1}{2}\exp\left(-\frac{I(I+1)}{2\sigma_\perp^2}\right)\exp\left(-K^2\left(\frac{1}{\sigma_K^2}-\frac{1}{\sigma_\perp^2}\right)\right)\right\}\rho_{state,np}(E, N, Z) \quad (9)$$

with

$$\sigma_\perp^2 = T\mathcal{J}_\perp.$$

3.3.3 Comparing spherical and deformed nuclei

On the basis of these Fermi gas expressions, one can see that even for neutron resonance reactions on even-even nuclei, investigating the level density of odd-N nuclei with angular momentum and parity $I^\pi = \frac{1}{2}^+$, one obtains a rotational enhancement, expressed as the ratio between the Ericson and Bethe formulas for the level density:

$$\frac{\rho_{Ericson}(E, N, Z, \frac{1}{2})}{\rho_{Bethe}(E, N, Z, \frac{1}{2})} \approx \frac{{\sigma_M}^3}{\sigma_K} = T\mathcal{J}_{sphere}\sqrt{\frac{\mathcal{J}_{sphere}}{\mathcal{J}_\parallel}} \approx T\mathcal{J}_\perp, \quad (10)$$

where the last approximation is valid for the nuclei studied here, with not too large deformations. For the neutron separation energy, this ratio will be about 50 for nuclei with mass number around 160.

As mentioned above, the ratio between the Bethe and the Ericson level densities cannot be investigated in experiments, and a more consistent procedure will be to compare state densities.

3.3.4 State densities for spherical nuclei and deformed nuclei

By evaluating the state density (1), inserting the Bethe level density (8), replacing sums by integrals, one comes back to the starting point, obtaining the state density of excitation of nucleons (2):

$$\rho_{state,Bethe}(E, N, Z) = \rho_{state,np}(E, N, Z). \quad (11)$$

This comes as no surprise: first, the Bethe level density is obtained by differentiating the state density with respect to the angular momentum. Then the Bethe state density is obtained by performing the inverse operation, namely integrating, bringing back the state density.

A more physical perspective on this connection between the level density and the state density may be given by relating back to symmetry properties. Summing the level density over all angular momenta, weighted with the degeneracy in a way corresponds to squeezing the nucleus, from the sphere on the lower right-hand side of fig. 1 into the irregular shape fixed in space, middle shape on the top row of fig. 1. All states will then appear as a separate level, with the possibility to be viewed in an experiment. For example, a neutron at low energy scattered on such an imagined fixed irregular nuclear shape, would couple to about a factor 10^3 more levels than when it scatters on a spherical even-even nucleus, where only the $I^\pi = 1/2^+$ levels are visible (inserting numbers for the $A \sim 160$ mass number region).

With the Ericson formula (9) for the level density of deformed nuclei, the state density (1) is obtained as a double sum over both the angular momentum I, weighted with the degeneracy $2I + 1$, and its projection K on the symmetry axis. Replacing sums by integrals, one ends up with

$$\rho_{state,Ericson}(E, N, Z) = \sigma_\perp^2\rho_{state,np}(E, N, Z). \quad (12)$$

In the Ericson picture, nucleons as well as the deformed rotor contribute to the level density. The extension by the phase space of the rotor yields a factor of $\sigma_\perp^2 = T\mathcal{J}_\perp$ more levels. This is consistent with the result obtained above for the ratio (10) between the Ericson and Bethe level density expressions.

4 Enhancement factor

4.1 Expectations based on fermi gas expressions

For deformed nuclei, one can evaluate the state density for nucleon motion (2), sampling levels [24,25] for general nuclear potentials (not just for the Fermi gas), by summing over *intrinsic states*, that is band-heads. Each band-head encompasses two intrinsic states, with projections K and $-K$ (except for the special $r = 0$ band-heads).

On the basis of the algebra just carried out for the Fermi gas level density for the Ericson formula, the ratio between the state density and the intrinsic state density is

then a measure of the rotational enhancement of the level density:

$$f_e = \frac{\rho_{state}}{\rho_{state,\,intrinsic}} \,. \tag{13}$$

For well-deformed nuclei with full rotational enhancement of the level density, one would expect the enhancement factor to be of the order of

$$f_e \approx T\mathcal{J}_\perp \quad \text{for well-deformed nuclei.}$$

For spherical nuclei, there are no band-heads. Instead internal states will display degeneracies of size $2I+1$, still yielding the state density for nucleonic motion (2) to be inserted as the intrinsic state density in the denominator of the expression for f_e. The numerator, the Bethe state density (11), is also equal to the state density for nucleonic motion (2), yielding

$$f_e \approx 1 \quad \text{for spherical nuclei.}$$

With these limiting values, it is apparent that for a Fermi gas, the enhancement factor f_e (13) is a measure of the amount of rotational enhancement of the level density.

4.2 SMMC and HFB

As suggested by Alhassid and coworkers, the rotational enhancement can quantitatively be expressed by the fraction f_e (13), evaluated on the basis of theoretical state densities.

The evaluations of f_e by Alhassid and coworkers are based on the full shell model with interactions. These interactions may induce correlations, including the ones which generate rotational bands. For the lowest temperatures, the SMMC is found to describe a thermal excitation of the lowest states for both of the nuclei, ^{148}Sm, with a vibrational-type band, and ^{154}Sm, with a typical rotational ground state band [3]. So, the SMMC procedure picks up the correlations present in the wave-functions by the random sampling procedure, without a priory information on the states. Applying the same spherical shell energies and the same interactions one can find the self-consistent HFB potential, which is deformed for rare-earth nuclei. For thermal excitations of the quasiparticles in the HFB potential, generated by Fermi-Dirac occupation probabilities, one can calculate the intrinsic level density for excitations in the deformed field implicitly present in the SMMC [2,3].

With increasing temperature of the occupation of quasiparticles in the HFB field, the nucleus undergoes a couple of phase transitions. First the pair fields of the HFB field weaken, and transitions to non-paired particle excitations occur, typically around 4–8 MeV of excitation energy. At higher energy, typically around 20–30 MeV for well-deformed nuclei, the single-particle HF field becomes spherical. Together with the transition to spherical shapes, the rotational enhancement fades away [2], eventually to approach the value $f_e \to 1$. Recently [4] the distribution of quadrupole deformation in SMMC has been documented carefully, displaying a characteristic development through the Samarium isotopes, from the transitional nucleus ^{148}Sm to the well-deformed nucleus ^{154}Sm.

4.3 FY and BCS combinatorial model

The present calculation is based on the combinatorial nuclear level-density model [25] using the Folded-Yukawa single-particle potential.

The radial shape of the Folded-Yukawa potential is chosen to match the overall relation between the nuclear density and the resulting potential at the nuclear surface. The parameters of the Folded-Yukawa potential are chosen such as to optimize nuclear masses [26]. Together with the masses, the equilibrium shapes of nuclei are also determined, and these will also be applied here.

The intrinsic states of the deformed potential are first calculated by constructing all many-particle-many-hole states in the potential. For each of these states, the quasiparticle structure is found, and BCS equations are solved to calculate the pair gaps. Each intrinsic state carries a projection K of the angular momentum on the symmetry axis, and is interpreted as a band-head, and a rotational band is built on top of each band-head. The contribution to the moment of inertia of protons and neutrons is given by the rigid-body moment of inertia times a reduction factor depending on deformation and pair-gaps [27]. The combinatorial level-density model based on the Folded-Yukawa potential and quasiparticle BCS theory is described in the paper by Uhrenholt *et al.* [25]. Further specific results are given in ref. [23].

Examples of the states obtained are given in the right-hand panels of figs. 2 to 4 of the present paper. On the basis of such results, the intrinsic state density is obtained just by counting band-heads, and the state density of the nucleus is obtained by counting all states within energy intervals. This presents a microcanonical ensemble, providing the numerator and denominator of the enhancement factor f_e (13).

4.4 Experimental data

Likewise, experimental intrinsic and overall state densities can be evaluated with microcanonical sampling, by counting experimental band-heads and states. Over the years, a vast amount of data on nuclear levels has been reported. These data are systematically evaluated (ENSDF) by the international network of "Nuclear Structure and Decay Data" evaluators [28]. Below we shall illustrate experimental band-heads and states (left-hand sides of figs. 2 to 4).

The evaluation of the enhancement factor f_e for experimental levels requires that rotational bands can be identified. The limit $f_e \to 1$, which should be obtained for decreasing deformation, cannot be explored for experimental levels, as we will discuss in connection to the "neglect band procedure" below.

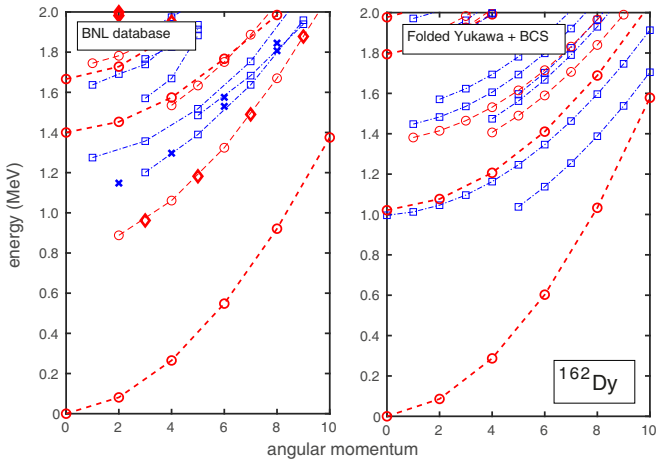

Fig. 2. Energies and angular momenta of low-lying nuclear states in the even-even nucleus ^{162}Dy. Left-hand side: bands and non-band levels according to the ENSDF Data base [28]. The data are fairly complete (accounting for more than about 90% of total states) within the whole energy and angular momentum interval shown on the figure [0–2] MeV × [0–10] $\hbar$. Right-hand side: band-heads calculated as many-particle-many-hole states with the Folded Yukawa potential and BCS pairing, supplied by rotational bands. The deformation of the potential is $\epsilon_2 = 0.25\,\epsilon_4 = -0.007\,\epsilon_6 = 0.019$. Circles connected by thick red dashes lines: $r = 0$ bands. Circles connected by thin red dashes lines: positive parity bands. Squares connected by thin blue dot-dashes lines: negative parity bands. Red diamonds: non-band positive parity levels. Blue crosses: non-band negative parity levels.

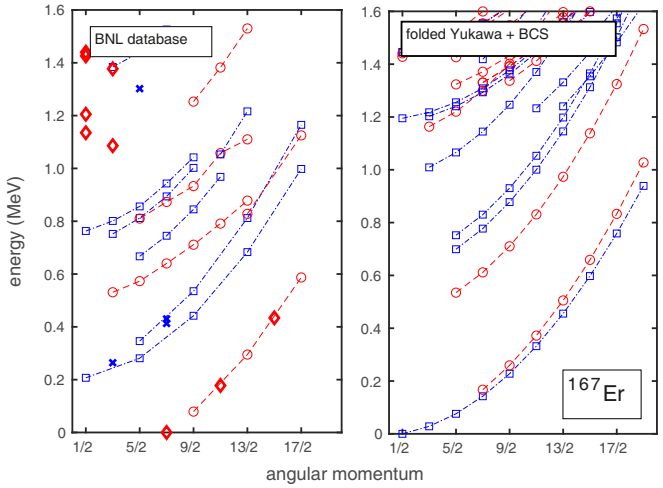

Fig. 3. Same as fig. 2, now for the odd-N nucleus ^{167}Er. The data on the left-hand side are fairly complete (accounting for more than about 90% of total states) within the energy and angular momentum interval [0–1.0] MeV × [1/2–13/2] $\hbar$ The deformation of the potential is $\epsilon_2 = 0.267\,\epsilon_4 = 0.027\,\epsilon_6 = 0.018$.

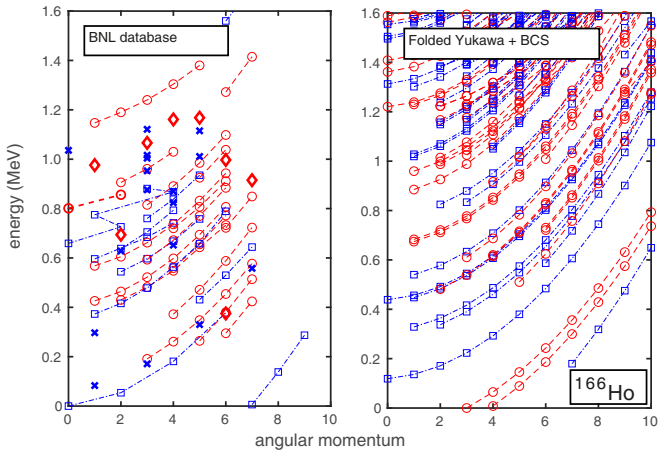

Fig. 4. Same as fig. 2, now for the odd-odd nucleus ^{166}Ho. The data on the left-hand side are fairly complete (accounting for more than about 90% of total states) within the energy and angular momentum interval [0–0.8] MeV × [0–6] $\hbar$ The deformation of the potential is $\epsilon_2 = 0.267\,\epsilon_4 = 0.020\,\epsilon_6 = 0.021$.

5 Statistics of low-lying levels and rotational bands

5.1 Band-heads and rotational bands

Figures 2 to 4 display experimental levels together with calculated, for an even-even, an odd-even and an odd-odd deformed rare-earth nucleus, respectively.

Glancing over the figures, one notices some general features:

- The figures clearly display an odd-even effect, with the density increasing from the even-even through the odd-even to the odd-odd. This is directly an effect of the pairing interaction.
- Just letting the eye follow the curvatures of the bands, comparing data and calculations, one sees that the calculated moments of inertia are quite realistic, when comparing to data.
- Several non-band states of the ENSDF compilation are actually located on bands, such as for example every second state on the ground-state band in ^{167}Er. This indicates that they belong to the band ($K^\pi = 7/2^+$), but the E2 gamma decay has not been recorded yet.

Looking in more detail, one may get an impression of how well the states calculated with the Folded Yukawa potential one by one compare to the data. Taking ^{167}Er as an example, the ground state has angular momentum and parity $I^\pi = 7/2^+$, and the first excited state around 200 keV of excitation energy has $I^\pi = 1/2^-$. With the Folded Yukawa potential, this order is the opposite.

Generally, for each experimental band in all three nuclei, one will find a calculated band within roughly 400 keV of energy. A few levels are more consistently missed, such as the 2^+ rotational band in ^{162}Dy, which is probably a band built on a γ-vibration.

5.1.1 Limitations in the data

In the present context, aimed at evaluating the intrinsic and overall state densities, it is important to consider the limitations of the data.

For the odd-odd nucleus ^{166}Ho, the bands do not stretch high up in angular momentum. This is probably due to constraints in the reactions studied, which do not populate high spin states. However, it may also be a sign of the vanishing of the rotational enhancement of the level density, that the bands actually are dissolving with increasing angular momentum.

For all three nuclei, one sees an increase of the occurrence of non-band levels with increasing excitation energy. This is probably due to i) the smaller intensity by which the higher lying states in energy are populated by the reactions, ii) the larger decay energies down to low-lying levels, making E2 transitions along a band less probable, and iii) the onset of mixing of rotational bands by the residual interactions, spreading out the full rotational strength of E2 transitions in such a way that the rotational enhancement of the level density is still valid, but it is difficult to identify band-heads and rotational bands. However, the increasing number of non-band levels may alternatively be seen as a sign of the gradual vanishing of the rotational enhancement of the level density, with particle-hole excitations exhausting the states of the deformed rotor, so that the rotational strength is actually lost.

With this reservation in mind, we continue to sample statistics for data as well as for calculations.

Table 1. The nuclei applied for sampling of level densities of counted levels and evaluation of the rotational enhancement factor. In the first row, the energy and angular momentum intervals of reliable experimental information is listed. In the second row, the ratio between experimental and calculated level densities close to the upper limit for the energy of counted experimental levels is given. The experimental numbers are evaluated on the basis of the data found in ENSDF [28]. In the third row, the ratio between experimental and calculated level densities at the neutron separation energy is given. Here, the experimental level density is directly taken from tables of the energy spacing of neutron resonances [31], and the calculated level densities are evaluated with a microcanonical sampling within a 100 keV wide interval over states of the same energy, parity and angular momentum as the states populated by s-wave neutrons.

odd Z	odd-odd
^{155}Eu, ^{171}Tm, ^{177}Lu,	^{166}Ho, ^{176}Lu, ^{182}Ta,
[0–1.0 MeV] $[\frac{1}{2} - \frac{9}{2}\,\hbar]$	[0–0.8 MeV] [0–6 $\hbar$]
$\langle \frac{\rho_{exp}}{\rho_{FY}}(0.8\,\mathrm{MeV})\rangle \approx 2.0$	$\langle \frac{\rho_{exp}}{\rho_{FY}}(0.6\,\mathrm{MeV})\rangle \approx 1.2$
$\langle \frac{\rho_{exp}}{\rho_{FY}}(S_n)\rangle \approx 6.0$	$\langle \frac{\rho_{exp}}{\rho_{FY}}(S_n)\rangle \approx 4.8$
even-even	odd N
^{156}Gd, ^{158}Gd, ^{162}Dy, ^{168}Er,	^{159}Gd, ^{161}Dy, ^{163}Dy, ^{167}Er
	^{171}Yb, ^{173}Yb, ^{175}Yb
[0–2.0 MeV] [0–6 $\hbar$]	[0–1.0 MeV] $[\frac{1}{2} - \frac{9}{2}\,\hbar]$
$\langle \frac{\rho_{exp}}{\rho_{FY}}(1.7\,\mathrm{MeV})\rangle \approx 1.0$	$\langle \frac{\rho_{exp}}{\rho_{FY}}(0.8\,\mathrm{MeV})\rangle \approx 1.6$
$\langle \frac{\rho_{exp}}{\rho_{FY}}(S_n)\rangle \approx 3.0$	$\langle \frac{\rho_{exp}}{\rho_{FY}}(S_n)\rangle \approx 3.8$

5.2 Average level density at low energy

In order to collect statistics, averages are carried out over a number of rare-earth nuclei. Von Egidy and Bucurescu have evaluated and tabulated the intervals in excitation energy and angular momentum over which the collected data concerning discrete levels can be considered fairly complete [29,30]. Within the mass region of interest here, 3 to 7 nuclei of each odd-even mass combination are selected. Table 1 gives the nuclei sampled with the intervals in energy and angular momentum.

First, the level densities of the different nuclei are simply summed, and an average level density is calculated for the four different even/odd combinations. The result is shown in fig. 5.

For this comparison, the summed level density over angular momenta is applied, that is without the degeneracy factor $2I+1$ entering in the state density (1). The summed level density does not have a direct physical significance. However, the choice of the conceptually more satisfactory state density would place too much emphasis on the higher angular momenta, for which the experimental information may be the most uncertain.

Figure 5 displays the overall increase of the level density expected, and it also shows that the Folded Yukawa plus BCS description agrees reasonably well with the overall trends of the data in the energy regions where data are available. However, the calculated level density is about a factor of 1.5 too small.

As illustrated in figs. 2 to 4, our calculated level density is based on band-heads of states in a prolate deformed potential with complete rotational bands added. This calculation of the level density is in accordance with the evaluation of the schematic Ericsson level density, given in sect. 3 of the present paper. Comparing the factor 1.5 to the enhancement factor (10) expected, which will be of magnitude 10 or higher, one may be tempted to conclude that the rotational enhancement is fully realized at these small excitation energies. However, this is a premature conclusion, and we shall proceed to explicitly evaluate enhancement factors.

5.3 Enhancement factors

The presence of experimental rotational bands with strong E2 transitions shows that the degrees of freedom of the deformed rotor contribute to the level density together with the nucleonic degrees of freedom. There is no other way of generating the strong E2 transitions. This also tells that the band-heads can be interpreted as intrinsic states and the intrinsic state density can be evaluated. Thus, the

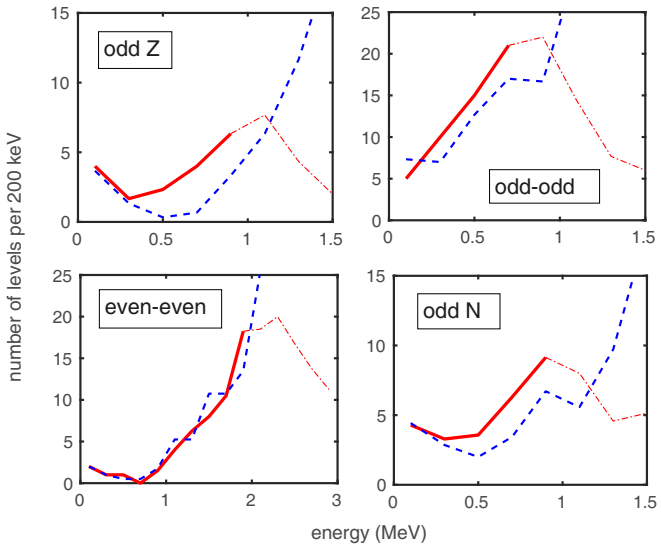

Fig. 5. The level density per 200 keV intervals summed over the angular momentum intervals and averaged over the nuclei listed in table 1 for the four even/odd combinations. Solid red curve: experimental levels in energy intervals where the information is fairly complete. Thin dot-dashes curve: experimental levels at energies with incomplete level schemes. Blue dashes curve: The calculated level density based on the Folded Yukawa potential with quasiparticle BCS pairing.

experimental states deliver the ingredients for evaluating the enhancement factor f_e (13).

The question is how to handle the non-band levels. Here, we include them as band-heads, which of course is questionable. For the evaluation of an experimental enhancement factor four prescriptions are applied:

- *Direct* application of the data from the ENSDF data base. Each non-band state counts as a band-head, with no addition of states on rotational bands.
- *Assigning* the non-band levels which clearly are located on bands to these bands, not counting them as band-heads. Both fig. 2 for ^{162}Dy and fig. 3 for ^{167}Er offer some examples of such states. This procedure of assigning to bands is the prescription which we find most satisfactory.
- *Completing* bands. One may take the naive view that all non-band states which are not located on bands are in fact band-heads, but the experimental limitations so far has not led to the discovery of the bands built on top of them. By hand one can then go on to add a whole rotational band on top of each non-band state, selecting a moment of inertia typical of the surrounding bands. Also, bands for which the experiment has only detected few states at low angular momentum, can be completed. When addressing the rotational enhancement, this by-hand completion of the data is very questionable, and it serves here to give an upper limit to the enhancement factor.
- *Neglect band procedure.* An equivalent lower limit to the enhancement factor is obtained by neglecting bands, that is counting all states as band-heads. One will then obtain an enhancement factor of the order of the average degeneracy of each level (divided by two since $+K$ and $-K$ are counted as two intrinsic states and only as one band-head). This yields a lower limit to the enhancement factor, being the average of $f_e \sim \langle (2I+1)/2 \rangle \sim 5$ for the current experimental levels. One may relate this to the limit $f_e \to 1$ for the *theoretical enhancement factor* which will appear for the case of pure nucleonic excitations without any collective states contributing to the phase space. In that case, all projections $M = -I, \cdots, I$ of a level with angular momentum I will contribute to the intrinsic state density. For the case of the interpretation of states as band-heads, only two states contribute to the intrinsic state density, $K = -I$ and $K = I$.

To achieve satisfactory statistics for the evaluation of enhancement factors, the data are sampled within only two energy intervals for the four even/odd combinations. The calculation based on the FY bands is then continued further up, to illustrate the general trend.

The result is displayed in fig. 6. The sampling of experimental states are within the following intervals: odd Z: 0–700 keV and 700–1100 keV, odd-odd: 0–500 keV and 500–700 keV, even-even: 1000–1500 keV and 1500–1900 keV, odd N: 0–600 keV and 600–900 keV. For the calculated states, these intervals are also used as the lowest two intervals for sampling, and the calculations are continued to higher energies with intervals of 400 keV width.

For even-even nuclei, the ground-state bands are not included in the evaluation.

The error bars on fig. 6 show the estimated uncertainty due to the sampling over rather few nuclei. The curves show the median, and the length of the error bar is the difference between 25% and 75% percentiles. For odd-Z, odd-odd and even-even, sampling by excluding one nucleus at a time is performed, giving three, three and four different samples, respectively. For odd-N, sampling over combinations of nuclei by excluding two at a time is carried out, resulting in 21 different samples. One sees that the error bars are rather small, and this allows for quoting typical results without reservation for sampling uncertainty.

5.3.1 Comparison experiment *versus* FY

Figure 6 shows that the calculations consistently overshoot the data, by about 40%. Even with the questionable completion of experimental bands, the FY calculations overshoot the data by about 20%. Making overall averages of data with the "assigning" procedure (solid red curves with error bars) and calculations (blue dashes curves) for both energy intervals and all four even/odd combinations, one obtains:

$$f_e = 17 \quad \text{experiment}, \tag{14}$$

$$f_e = 23 \quad \text{calculations}, \tag{15}$$

and one notes that the absolute lower limit to the enhancement obtained with the "neglect band" procedure, (thin

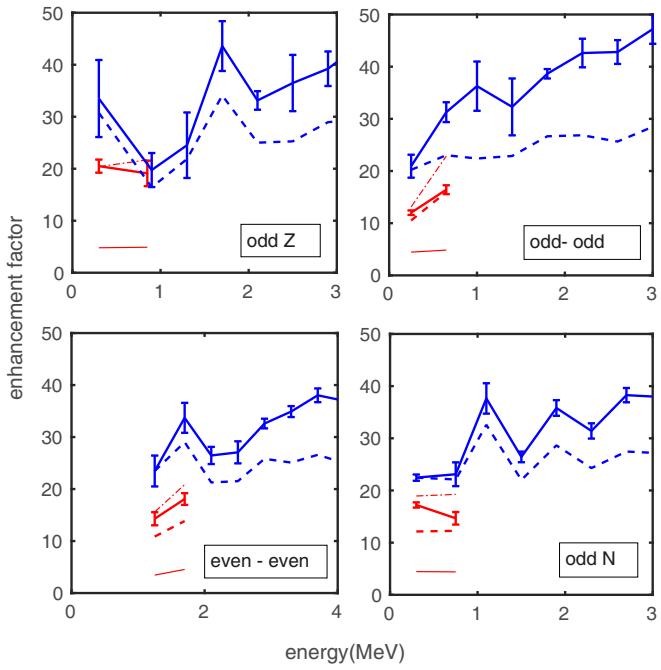

Fig. 6. Enhancement factors of the four even/odd combinations of nuclei, obtained by sampling band-heads and states within energy intervals typically 400 keV wide. Red lines: Experimental values obtained by applying different procedures for identifying band-heads and rotational bands, as explained in the text. Thin red lines: "neglect band" band procedure. Red dashes: "direct" procedure. Red solid line with error bars: "assigning" procedure. Red dot-dashes line: "completing" procedure. Blue lines: Enhancement factors based on the Folded Yukawa plus BCS calculations. Blue dashes: Summation over angular momenta restricted to the same interval as for the experimental levels —that is including angular momenta 1/2 to 19/2 for odd mass nuclei and 0 to 9 for even mass nuclei. Solid blue lines: Unrestricted summation over angular momenta. The error bars displayed for two of the curves are associated with the rather small samples of nuclei, as explained in the text.

red curve) yields the average $f_e = 5$, which is well below the experimental as well as the theoretical value.

We have not found any straightforward explanation of this difference between the experimental and theoretical results

From the Fermi gas expressions, the enhancement factor is the product of the temperature and the moment of inertia, and fig. 6 roughly confirms the expectation that the enhancement should increase as function of excitation energy, however overlayed with substantial irregularities.

From figs. 2 to 4 one gets the impression that the moments of inertia of the calculations roughly correspond to the experimental ones, and this is confirmed by more quantitative evaluations.

One may ask whether the experimental bands gradually loose their collectivity, which would show up as generally decreasing moments of inertia along the single bands with increasing angular momentum. For the nuclei studied, the moments of inertia are found to stay fairly constant, typically gradually decreasing or increasing within

Table 2. State densities (MeV^{-1}) and average square angular momenta ($\hbar^2$) from calculations and data for the nucleus ^{162}Dy at excitation energy $E = 1.9$ MeV. The SMMC and HF results are read off from figures in ref. [3]. Especially, the temperatures $T = 0.261$ MeV and $T = 2.70$ MeV are determined from fig. 6 in ref. [3] to represent $E = 1.9$ MeV for SMMC and HF, respectively. The FY and data results are obtained by sampling levels within the energy interval 1.8–2.0 MeV, displayed in fig. 2, including also levels at higher angular momentum (one level for both data and FY results). Error bars on the theoretical results, due to parameters and randomness of the sampling, are estimated to be around 20%.

^{162}Dy $E = 1.9$ MeV	ρ_{state}	$\rho_{state,\,intrinsic}$	$\langle J^2 \rangle$	$\langle K^2 \rangle$
SMMC, HF	1970	260	64	16
FY, BCS	1315	65	60	6.6
data	1345	50	60	6.4
FY, no pairing	28300	650	86	16.4

only 10%. In that respect, they recall the ground-state bands and other specific bands investigated in the early studies of rotational nuclei, as expressed in the smallness of the term $BI^2(I+2)^2$ contributing to the rotational energy [32].

Together with the large E2 matrix elements for decay along the bands, this regular behavior of the rotational energy along each bands also gives credibility to the evaluated experimental enhancement factor (14), that the deformed rotor really contributes with that factor to the phase space of nuclei at these low excitation energies.

5.3.2 Comparison SMMC *versus* FY

A comprehensive discussion of thermal properties and level densities calculated with the SMMC and HFB theories has been carried out by Alhassid, Bertsch *et al.* [3]. Especially, results are given for the well-deformed nucleus ^{162}Dy, which is among the nuclei studied here, and illustrated in fig. 2.

From figures in ref. [3], one can extract numbers for level densities and moments of the distribution of angular momentum, which may shed light on the different approaches to evaluating the level density. We here take the highest energy interval in ^{162}Dy, for which reliable data exist, 1800–2000 keV, represented by the energy 1900 keV. The relevant numbers are collected in table 2.

From the SMMC and HF results, one obtains an enhancement factor (13) of around 8, which is also typical of the values shown for the two deformed nuclei ^{152}Sm and ^{154}Sm [2] at the low excitation energies.

In ref. [3], the results for ^{162}Dy are evaluated without pairing in the Hartree-Fock field, and this seems somewhat surprising, considering the pronounced gap in the spectrum from the ground state to the first excited state, shown in fig. 2. The HF intrinsic state density should act as a prediction of the experimental intrinsic state density,

and it fails in this respect. With the inclusion of pairing, the calculated intrinsic state density with HFB would attain a much lower value, of about the same magnitude as the data or the FY values, and the enhancement factor would be of the same order as the experimental value.

6 Level density at the neutron separation energy and above

To complete the discussion of the level density of discrete identified nuclear states, let us look at the comparison between data on the level density at the neutron separation energy, and the predictions by the FY calculations. A general comparison was carried out in ref. [25], and we shall limit ourselves to the different even/odd combinations of mass number given in table 1, for which the data at low energy were the most complete.

The factor 1.5 for the ratio between experimental and calculated level densities at the top of the interval of resolved states increases to about a factor of 4.5 at the neutron separation energy.

The FY level density includes a rotational enhancement factor of $f_e \approx 50$, and still it is smaller than the experimental level density. On this basis, there is no sign of fading away of the rotational enhancement at the neutron separation energy for these well-deformed nuclei.

To follow up on the discussion of the previous section, we may focus on the situation for the nucleus ^{162}Dy, comparing to the SMMC and HF results [3]. For this nucleus, the FY calculations underpredict the experimental level density at the neutron separation energy by a modest factor of 2.2. The SMMC calculations predict the data precisely, and the HF without pairing and with rotational bands supplied overpredicts the data by about a factor of 5. Without pairing, the FY calculations would overpredict the level density at the neutron separation energy by a factor of 4. (All of these factors come with an uncertainty of about 20%).

Still, for the nuclei taken together, the factor 4.5 between the data and the FY results clearly indicate that a contribution to the level density is missing.

6.1 Vibrational enhancement

The extension of the phase space with the degrees of freedom of surface vibrations may provide these missing factors to the combinatiorial level density, that is a *vibrational enhancement* of the level density. And the problem of *overcounting* becomes relevant. Concerning the present combinatorial level density based on the Folded Yukawa potential, a negligible enhancement due to vibrations was found. At the neutron separation energy, the vibrational degrees of freedom were already accounted for by nucleonic excitations [25].

An opposite view on this is suggested by Goriely and co-workers [24], who extend the phase space of nucleonic excitations by bosons of multipolarity up to and including $\lambda = 4$, and with up to maximally three phonons in each vibration. This leads to an appreciable vibrational enhancement of the level density. However, neither two-phonon states nor three-phonon states have systematically been observed in nuclei, and such observations seem to be required for an overall inclusion of these degrees of freedom in the phase space. One may quote the results shown in reference [24] for the nucleus ^{176}Lu, which is one of the nuclei studied here. For this nucleus, vibrational enhancement factors are displayed, of magnitude $f_{e,vib} \approx 2$ at 0.7 MeV, and $f_{e,vib} \approx 10$ at the neutron separation energy of 6.4 MeV. These numbers may be compared to the missing contributions to the FY level density of 1.5 for counted levels and 4.5 at the neutron separation energy, respectively.

Concerning the vibrational enhancement, one may note that for deformed nuclei, the phonons carry angular momentum quantum numbers relevant for the strong coupling scheme. In this way, the vibrational enhancement contributes to the intrinsic as well as to the overall state density. Thus, the vibrational enhancement would not be explored by the enhancement factor f_e (13) inserting experimental states.

However, in shell model calculations, the full shell model, represented by SMMC, may contain both rotational and vibrational correlations in the states, and a comparison with mean field quasiparticle calculations, such as HFB, will reveal both types of enhancement. For the transitional nucleus ^{148}Sm, the SMMC *versus* HFB calculations of the enhancement factor is referred to as vibrational enhancement [2], motivated by the vibrational character of the ground-state band. For well-deformed nuclei, the enhancement factor should account for vibrational as well as rotational enhancement.

6.2 Experimental searches for fade-out of enhancement

We have already mentioned in sect. 2 the negative result obtained in the experiment by Komarov *et al.* [15] aimed at identifying the fade-away of the rotational enhancement around excitation energies 30 to 60 MeV. It may be that one should also look at somewhat lower excitation energies.

Based on the evaluations by SMMC one should expect the rotational enhancement to fade away around 20–30 MeV of excitation energy [2–4], and the vibrational enhancement is assumed [24] to fade away in the interval around 10–20 MeV of excitation energy.

Spectra of evaporated neutrons from nuclei at excitation energies from 10 to 40 MeV should be ideally suited for this study, and recent experiments by Banerjee *et al.* and by Pandit *et al.* [33,34] address this question. The slope of the evaporation spectrum is essentially given by the inverse temperature of the level density in daughter nuclei. A loss of collective enhancement of some kind will reflect itself in a systematic behavior of the temperature around some energy interval, preferably a temperature inversion, and such behavior has been reported [33].

It seems that in both the experiments [33,34] enhancement factors of the order of 3 to 10 appear within a rather narrow energy interval of about 5 MeV width, and then fade away. This could be a probe of the fading away of vibrational enhancements.

However, the restriction to narrow intervals is not what is expected for the types of enhancement considered here, caused by collective degrees of freedom. The contribution of such degrees of freedom to the level density will set in from the smallest excitation energies, then increase with increasing excitation energy, to reach some maximum and then fade away. Clearly, it is difficult to disentangle such behavior from effects of the gradual weakening of shell structure, and the gradual weakening of the pair field, which may manifest itself through a constant temperature within a certain excitation energy interval [35].

In view of this, it seems to us that the interesting results [33,34] reported by Banerjee *et al.* and by Pandit *et al.* cannot at present be given a clear interpretation

7 Conclusion

Applying schematic Fermi gas expressions, the relation between the symmetry of the nuclear shape, and the level density is highlighted. Especially, it is shown how the phase space of nucleonic excitations for deformed nuclei is greatly extended via the degrees of freedom of a deformed core, giving rise to the rotational enhancement of level densities.

The main result of the present paper is a thorough analysis of the enhancement factor at the lowest excitation energies in the 17 deformed rare earth nuclei, where the experimental information is most complete. Results from the combinatorial level density model based on the Folded Yukawa potential with BCS quasiparticle pairing are presented and compared to data, first with respect to the moments of inertia of rotational bands and the sequence of levels. An average theoretical enhancement factor of $f_e = 23$ is found, and the equivalent average experimental factor is evaluated to be $f_e = 17$. On this basis, it is concluded that the full rotational enhancement exists for these low-lying states, in accordance with the original discussion by Bjørnholm, Bohr and Mottelson.

However, around the neutron separation energy, the combinatorial FY model level density undershoots the data by a factor of about 4.5. This may be a sign of vibrational enhancement, that is a contribution of low-lying surface vibrations to the phase space. In this connection, is important that the full SMMC calculations precisely predict the correct level density at the neutron separation energy.

Finally, we have qualitatively discussed the situation at higher excitation energy, by quoting different experimental results. Recent experiments may have observed some weakening of the vibrational enhancement.

It seems to us that large-scale shape fluctuations may be the answer to some of the results observed at higher energies, showing no fade-away of the enhancement.

Inclusion of large-scale shape fluctuations in SMMC calculations would require single particle high-j orbitals from shells above the Fermi energy to enter the phase space.

Data Availability Statement This manuscript has no associated data or the data will not be deposited. [Authors' comment: All data generated during this study are contained in this published article.]

References

1. P.F. Bortignon, R.A. Broglia, Nucl. Phys. A **371**, 405 (1981).
2. A. Ozen, Y. Alhassid, H. Nakada, Pys. Rev. Lett. **110**, 042502 (2013).
3. Y. Alhassid *et al.*, Phys. Rev. C **93**, 044320 (2016).
4. M.T. Mustonen, C.N. Gilbreth, Y. Alhassid, G. Bertsch, Phys. Rev. C **98**, 034317 (2018).
5. V. Zelevinsky, M. Horoi, Prog. Part. Nucl. Phys. **105**, 180 (2019).
6. H.A. Bethe, Phys. Rev. **50**, 332 (1936).
7. H.A. Bethe, Rev. Mod. Phys. **9**, 69 (1937).
8. T. Ericson, Adv. Phys. **9**, 425 (1960).
9. S. Bjørnholm, A. Bohr, B. Mottelson, *Physics and Chemistry of Fission*, *Proceedings of a Conference at Rochester*, Vol. **1** (IAEA, Vienna, 1974) p. 367.
10. T. Døssing, A.S. Jensen, Nucl. Phys. A **222**, 493 (1974).
11. J.R. Huizenga *et al.*, Nucl. Phys. A **223**, 577; 589 (1974).
12. S.T. Belyaev, V.G. Zelevinsky, Yad. Fiz. **11**, 741 (1970) (Sov. J. Nucl. Phys. **11**, 416 (1970)).
13. S. Karampagia, A. Renzaglia, V. Zelevinsky, Nucl. Phys. A **962**, 46 (2017).
14. G. Hansen, A.S. Jensen, Nucl. Phys. A **406**, 236 (1983).
15. S. Komarov *et al.*, Phys. Rev. C **75**, 064611 (2007).
16. K.-H. Schmidt, J.G. Keller, D. Vermeulen, Z. Phys. A **315**, 159 (1984).
17. A.R. Junghans *et al.*, Nucl. Phys. A **629**, 635 (1998).
18. A. Bohr, B.R. Mottelson, *Nuclear Structure*, Vol. **I** (Benjamin, Reading, MA, 1969).
19. S. Åberg, Nucl. Phys. A **477**, 18 (1986).
20. O. Andersen *et al.*, Phys. Rev. Lett. **79**, 687 (1979).
21. T. Døssing *et al.*, Phys. Rep. **268**, 1 (1996).
22. S. Leoni *et al.*, Phys. Rev. C **72**, 034307 (2005).
23. S. Åberg *et al.*, Nucl. Phys. A **941**, 97 (2015).
24. S. Goriely *et al.*, Phys. Rev. C **78**, 064307 (2008).
25. H. Uhrenholt *et al.*, Nucl. Phys. A **913**, 172 (2013).
26. P. Möller *et al.*, *Atomic Data and Nuclear Data Tables* LA-UR-15-26310 (2015).
27. R. Bengtsson, S. Åberg, Phys. Lett. B **172**, 277 (1986).
28. ENSDF data base, interface NuDat, searched for the present evaluation in the interactive nulear chart: `www.nndc.bnl.gov/nudat2/`, data checked April 2019.

29. T.v. Egidy, D. Bucurescu, Phys. Rev. C **78**, 051301(R) (2008).
30. T.v. Egidy, D. Bucurescu, Phys. Rev. C **80**, 054310 (2009).
31. RIPL3, Rererence Input Parameter Library, IAEA-Tecdoc, 2009, available at `http://www-nds.iaea.org/RIPL-3/`.
32. A. Bohr, B.R. Mottelson, *Nuclear Structure*, Vol. **II** (Benjamin, Reading, MA, 1975).
33. K. Banerjee *et al.*, Phys. Lett. B **772**, 106 (2017).
34. D. Pandit *et al.*, Phys. Rev. C **97**, 041301(R) (2018).
35. L.G. Moretto *et al.*, J. Phys. Conf. Ser. **580**, 012048 (2015).